Production of VO_2 M_1 and M_2 Nanoparticles and Composites and the Influence of the Substrate on the Structural Phase Transition

Jamie M. Booth* and Philip S. Casey

CSIRO Materials Science and Engineering, Private Bag 33, Clayton South, Victoria 3169, Australia

ABSTRACT A two-step, high-purity, high-yield synthesis of nanoparticulate vanadium dioxide, which has a greater than 10-fold potential cost reduction is reported. This consists of a short reflux of V_2O_5 with aspartic acid, followed by calcination at 600 °C or above. The particles produced have a mean diameter of approximately 90 nm with phase change characteristics of transition temperature and enthalpy that compare favorably with a commercial standard. In cases where the reduction reaction has progressed too far and a mixture of vanadium(III) and -(IV) is formed, redispersion and aging of the particulate product in water preferentially oxidizes the vanadium(III) component to vanadium(IV), thus allowing a versatile route to achieving a high-purity material. The synthesis was also used to deposit high-purity phases of VO_2 onto the surfaces of other particles, and significant differences in the structural phase transition behavior and even the crystal structure were found for deposited samples. The data suggest that substrate properties may affect the characteristics of the structural phase transition, and this has significant implications for measurements on, and applications of, deposited VO_2 layers and films.

KEYWORDS: VO_2 • nanoparticles • multifunctional • thermochromic • aspartic acid

INTRODUCTION

Materials that are able to switch a particular intrinsic property in response to an extrinsic stimulus are of significant interest to materials scientists for reasons that are self-evident. Of particular interest is vanadium(IV) oxide because one of its many stable polymorphs, $VO_2(M_1)$ (1, 2) with space group $P2_1/c$ (No. 14), undergoes just such a transition near room temperature. As the ambient temperature exceeds 68 °C, it changes its electronic character from a semiconductor to a metal as its crystal structure changes from monoclininc $P2_1/c$ (No. 14) to tetragonal $P4_2/mnm$ (No. 136). There is still much debate about the driving forces of the transition however. While there is significant evidence for a Peierls-type transition in which the crystal structure change resulting from softening phonon modes results in the breaking of the band symmetry (3, 4), there also exists equally significant evidence for electron−electron correlations, rather than electron−lattice correlations, changing the band structure (5−7). In recent years, studies have found that the actual mechanism may be analogous to the coupled Mott−Peierls mechanism, in which both effects are active (8, 9); however, this explanation is still unable to account for all observed phenomena (10).

Recent X-ray absorption fine structure spectroscopy (XAFS) data, however (11), suggest that significant expansion of the monoclinic unit cell occurs in the [110] and [1$\bar{1}$0] directions of the high-temperature rutile unit cell across the transition. This expansion propagates via apical oxygen atoms of the octahedra to the neighboring sublattice and induces a strain on the Peierls paired V−V bonds along the rutile *c* axis. A very similar stress-induced strain resulting in depairing of the vanadium ions was reported by Pouget et al. (12), who applied uniaxial stress along the [110] direction of the rutile cell and found it to result in the formation of the transitional M_2 structure. This VO_2 polymorph possesses $C2/m$ (No. 12) symmetry (2, 4, 12), corresponding to a structure in which only one of the two edge-sharing chains undergoes Peierls distortion. Therefore, the stress results in depairing of the vanadium cations. The same XAFS data (11) also found that the mechanism by which the doping of VO_2 with tungsten lowers the phase transition temperature is also due to just such a stress, generated by the larger covalent radii of the tungsten ions resulting in expansion in the [110] and [1$\bar{1}$0] directions of the rutile unit cell. Therefore, recent work suggests that stresses generated by phonon hardening are intrinsic to the structural phase transition, with less recent work indicating that externally applied stresses can also have a significant effect on the phase transition.

According to another recent study (4), the transition from tetragonal to monoclinic can be identified with two soft phonon modes that "describe two independent Peierls distortions along chains of edge sharing octahedra". Mapping of the free energy over the space spanned by these two phonon modes reveals saddle points intermediate to the high-temperature VO_2(R) phase and minima corresponding to the low-temperature $VO_2(M_1)$ phase. These saddle points were identified as the $VO_2(M_2)$ structure. Parts a−c of Figure 1 illustrate the differences between these three VO_2 structures.

The subsequent band structure changes associated with the insulator−metal transition create electronic transitions to the conduction band that fall into the near-infrared (13),

* E-mail: jamie.booth@csiro.au.
Received for review May 12, 2009 and accepted August 18, 2009

DOI: 10.1021/am900322b

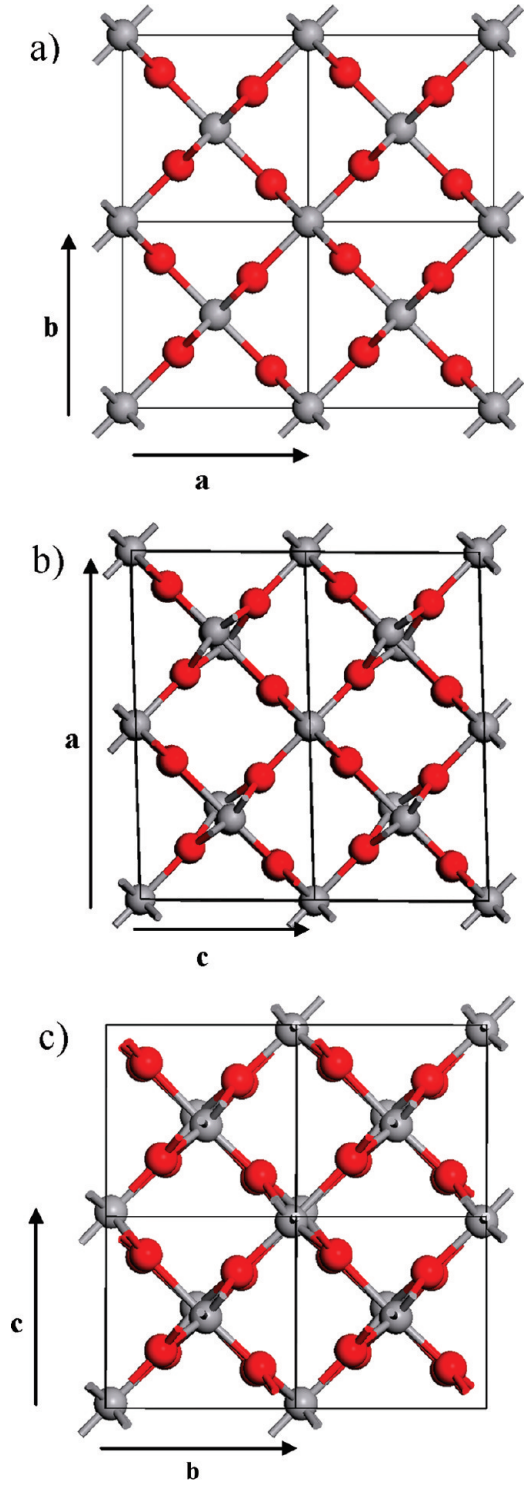

FIGURE 1. Identical perspectives of the (a) R, (b) M_2, and (c) M_1 structures of VO_2 illustrating the changes in the transition from the high-symmetry R phase to the M_2 structure in which every other chain of octahedra is Peierls distorted to the M_1 phase in which both chains of octahedra are Peierls distorted.

creating temperature-dependent spectral properties with a significant potential for applications such as thermochromic glazing (14, 15) and near-infrared optical switches (16). The increase in the electronic conductivity of the material can be up to 5 orders of magnitude (13), resulting in the potential for temperature-dependent electrical switching devices. It is this potential that motivates the vast majority of the current applied research into VO_2. To realize its potential in applications, it is essential that methods capable of producing "convenient for use" VO_2 are developed and exploited. Commercially available forms of VO_2 are expensive and limited to bulk powders of large primary particle size. These limitations significantly hinder extensive research and development programs, and to date, much of the considerable potential of VO_2 is latent.

Literature syntheses of vanadium dioxide fall into one of three groups: (i) chemical vapor deposition (CVD) routes to produce thin films for glazing purposes (14, 15) and nanowires (17), (ii) sol–gel deposition via dip-coating, followed by calcination for similar applications (18, 19), or (iii) precipitation of an amorphous vanadium(IV) precursor from solution, followed by calcination to produce small particles or nanopowders (20–22). Each of these approaches is limited in that they only produce either films or powders. CVD routes require stringent controls at elevated temperatures and are susceptible to the consequences of temperature gradients. Reactor and delivery systems are expensive to set up on a large scale, and their use is predominantly limited to producing films. Similarly, sol–gel deposition methods based on alkoxides of vanadium (18, 19) or vanadium acetylacetone (23) have been used to produce thin films of VO_2, but the precursors are both chemically sensitive and expensive. Deposition of a vanadium(V) precursor followed by a subsequent reduction to vanadium(IV) using a reductant gas such as hydrogen may be feasible (24) but is technically demanding and again only produces films.

A single process flexible enough to produce coatings, films, and/or powders has a substantial advantage over the synthesis methods outlined above, particularly if it can reduce equipment and reagent inventories, avoid the elevated temperatures typically used in CVD, and allow greater flexibility in application. This may include, for example, its direct use as a functional (and nano) additive in polymeric films and coatings or the production of composite multifunctional additives using a functional carrier substrate particle. In the latter, organic molecules may be used to tether the vanadium precursor compound to the substrate surface. Consequently, the production of coated or thermoformed large-area components incorporating VO_2 for application may be produced and, by avoidance of the elevated temperatures required by CVD and its lack of transportability, provide the possibility of coating temperature-sensitive substrates such as plastics, wood, etc., in unconstrained working/production environments, thus greatly expanding the scope of potential applications.

The study described herein uses aspartic acid in a manner similar to that recently reported for gold nanoparticles (25) to develop a simple synthetic route to produce VO_2, with the versatility of producing either particles directly or by surface deposition on a range of substrates (in this study, clay and silica). The synthesis is extremely facile and produces nanoparticles and composites of high purity, with a possible 10–15-fold cost reduction over commercially available bulk VO_2. However, we find that the nature of the substrate

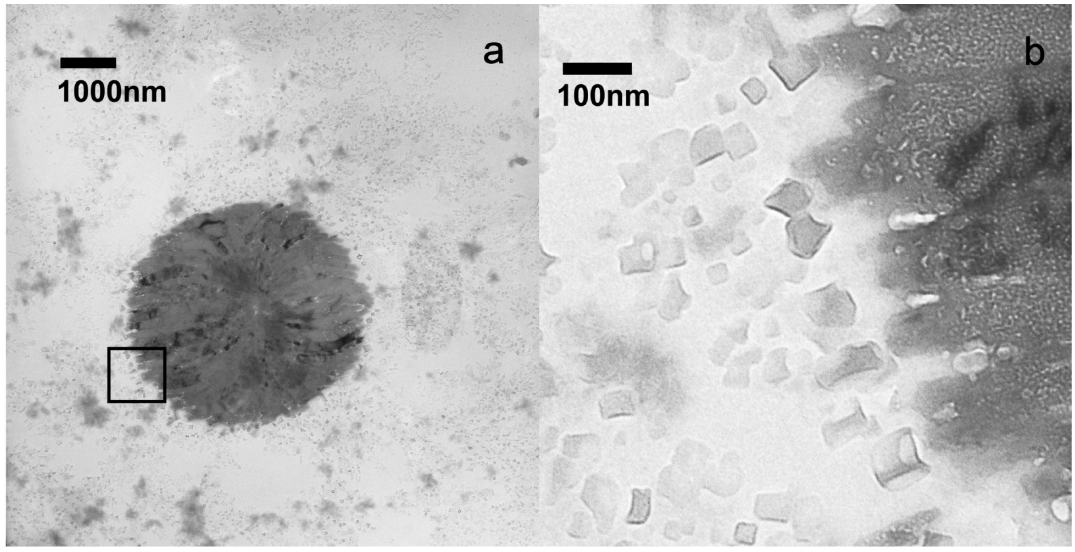

FIGURE 2. TEM images of a gel-like cluster formed from the reflux of aspartic acid and V_2O_5. The rectangle of part a marks the area imaged in part b.

significantly affected the properties of the deposited VO_2, with deposition onto montmorillonite, in particular, resulting in the formation of the M_2 structure rather than M_1 VO_2. Given the intense theoretical (7) and commercial (13, 14) interest in deposited VO_2 films, the results presented here suggest that considerable care must be taken to either account for or avoid VO_2—substrate interactions.

MATERIALS AND METHOD

The expected oxidation product of aspartic acid, 2-oxoethanoic acid (26), is chemically simple and physically small and, therefore, less likely to stabilize the reduced vanadium product in solution; thus, the product is more likely to precipitate/deposit readily. Because the amino acid is expected to bind readily to the transition metal oxide (26, 27), vanadium pentoxide dissolution is unnecessary and simply refluxing it with amino acid is sufficient to form the cross-linked VO_2 precursor. Furthermore, both starting materials, aspartic acid and V_2O_5, are readily available and relatively inexpensive.

Pure Vanadium Dioxide Synthesis Method. A 2 h reflux of 0.9 or 1.0 g of vanadium pentoxide (Riedel de Haan) with 1.0 g of aspartic acid (Aldrich) in 50 mL of water purified with a Milli-Q filter was employed to reduce vanadium(V) oxide to a vanadium(IV) precursor. The resultant precipitate was filtered, washed with water, dried, and then calcined under argon in a tube furnace at 600 or 800 °C for either 1 or 8 h. Yields calculated after calcination were typically >80%.

Vanadium Dioxide Composite Production. A total of 1.5 g of aspartic acid was first refluxed with either 0.1 g of montmorillonite (Sodium Cloisite, Southern Clay Products) for 1 h or 0.05 g of fumed silica (Cab-O-Sil, Degussa) for 20 min. Then 1.0 g of vanadium pentoxide was added and the mixture refluxed for a further 6 h for the montmorillonite composite or 4.75 h for the silica composite. The silica composite was filtered off immediately after the reflux step, dried, and calcined at 800 °C under argon for 8 h. The montmorillonite composite precipitate was centrifuged off, redispersed in water for 18 h, then filtered, dried, and calcined under argon in a tube furnace at 800 °C for 1 h because no difference was observed between the structure and phase transition dynamics of samples calcined for either 1 or 8 h. A temperature of 800 °C was used because it is above the melting point of V_2O_5 and therefore encourages any residual V_2O_5 to separate from any VO_2 formed. However, the reaction conditions reported here have been optimized such that this separation was not apparent for the samples analyzed below.

X-ray Diffraction (XRD). A Bruker D8 Advance using Cu Kα radiation was employed to acquire the diffraction spectra of the samples.

Transmission Electron Microscopy (TEM). The samples were deposited on 200 mesh carbon-coated copper grids, and microscopy was performed on a Philips CM30 transmission electron microscope operating at an accelerating voltage of 200 kV.

Differential Scanning Calorimetry (DSC). Calorimetry experiments were performed on a Perkin-Elmer Pyris 1 calorimeter using hermetically sealed aluminum pans, between 20 and 100 °C at a scan rate of 5 °C/min under nitrogen.

Voltammetry. The sample was decanted from the reflux setup and water-cooled to 20 °C in a jacketed electrochemical cell. Rotating-disk electrode (RDE) voltammetry was then performed using a glassy carbon electrode rotating at 2000 rpm and a carbon counter electrode measured against an Ag/AgCl reference electrode controlled by a Gamry PCI 4G750-42067 electrochemical analyzer. The sample was then reintroduced to the reflux setup.

RESULTS AND DISCUSSION

Pure VO_2 Powder. Parts a and b of Figure 2 display the TEM images of a typical sample during the redox process. Clearly visible (Figure 2a) is a large cluster of high-electron-density material that does not exhibit any order upon inspection of its electron diffraction pattern and thus is not V_2O_5, which possesses an orthorhombic structure. The high density of the cluster suggests that it is not a polymeric form of amino acid. Therefore, amino acid binds to the vanadium species of V_2O_5 via chelation by the glycyl group and complexation by the carboxylic acid groups at the other end of the molecule (26, 27) (a singly connected amino acid cannot act as a cross-link), thereby forming an extended gel-like structure.

By chelation of V_2O_5 into the gel-like structure, aspartic acid becomes more "soluble" because it transforms from an insoluble solid to a far less rigid and more accessible

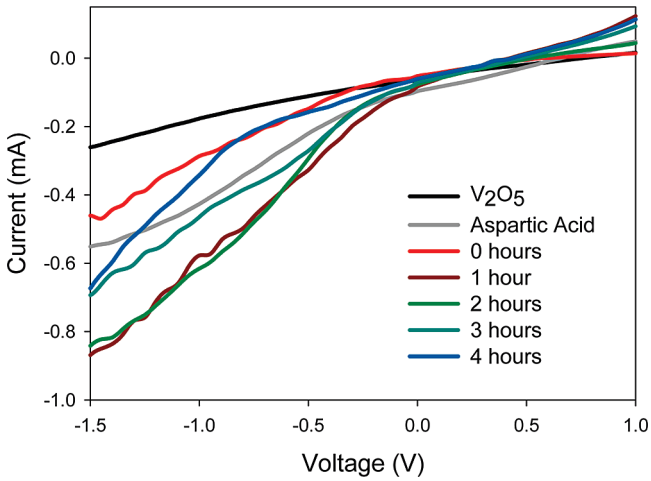

FIGURE 3. RDE data of a refluxing sample of 1:1 (w/w) V_2O_5 and aspartic acid at intervals of 1, 2, 3, and 4 h, compared with pure V_2O_5 and aspartic acid in water.

semisolid. RDE voltammetry experiments (Figure 3) on a 1:1 (w/v) 0.11 M in V_2O_5 and 0.15 M aspartic acid show a significant increase in the current during the first 2 h of reflux, compared to currents in slurries of V_2O_5 and aspartic acid, both individually and combined. The combined slurry exhibits currents approximately intermediate between V_2O_5 and aspartic acid because of high concentrations of both reactants, resulting in the inhibition of aspartic acid transport to the electrode surface. This increase in the current at early reaction times suggests a greater reactivity at the RDE surface arising from the conversion of the solid starting powders into more soluble species. Consumption of this species results in a decrease in reducible species illustrated by the reduction of the current at negative voltages. However, a concurrent increase in the current at positive voltages suggests the formation of a new, oxidizable species: vanadium(IV).

The cluster extremities exhibit regions of comparable electron density that appear to be detaching from the cluster (see Figure 2b). The oxidation of aspartic acid by a transition-metal cation is expected to proceed via chelation of the cation by the glycyl group of amino acid. Reduction of the metal ion is accompanied by the formation of an oxygen radical from the carbonyl group of the acid and detachment of the reduced metal species, as illustrated in Scheme 1 (26). The detachment illustrated in the TEM image suggests the manifestation of a similar reaction mechanism: Oxidation of amino acid produces an oxygen radical, resulting in acid decomposition as the radical decays through a further redox reaction, reducing another metal species to an amine carbocation, which itself decays into 2-oxoethanoic acid and an ammonium ion.

Evidence of a two-electron donation process by amino acid can be obtained from the reaction stoichiometry. For a typical reaction involving 1 g of V_2O_5 and 1 g of aspartic acid, the ratio of aspartic acid to vanadium atoms is approximately 0.68, which is insufficient for complete conversion to VO_2 in a single-electron process. In our experiments, the average yields of VO_2 after calcination are greater than 80%

Scheme 1. Generalized Mechanism of Aspartic Acid Oxidation by a Metal Cation, Based on the Work of Sherigawa et al. (*26*)

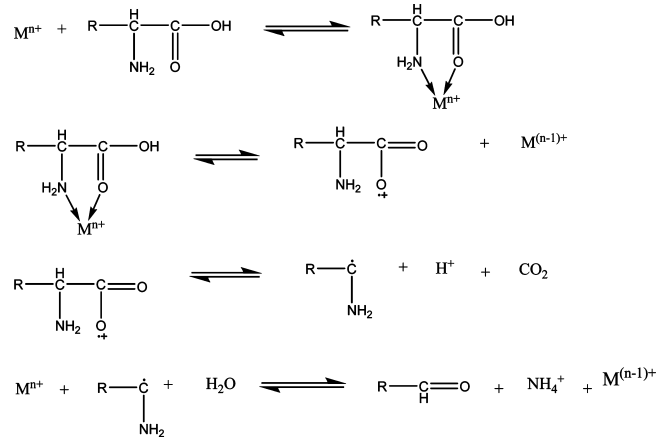

and sometimes 90%, and for such yields to be possible, a two-electron process must occur.

The XRD pattern of the dried precipitate of a sample in which the redox reaction has not reached completion (see Figure 4) exhibits some low-intensity diffraction peaks that index to $(NH_4)_2V_{10}O_{25}\cdot 8H_2O$. Because ammonia was not present, the reaction stoichiometry suggests that the most likely source for the formation of ammonium ions that charge balance the two vanadium(IV) ions is from the reaction mechanism illustrated in Scheme 1. It is possible, however, that the nonglycyl carboxy group is also oxidized given that these groups must be binding to vanadium ions. A corollary of this is that, upon substitution of asparagine (two amino groups) for aspartic acid, a gel-like structure was formed. In this case, however, the redox reaction rate was extremely slow and a vanadium(IV) oxide precipitate did not form, implying that the low-density networked structure was quite stable. Therefore, the redox reaction mechanism in these systems seems to be a combination of that proposed by Sherigawa et al. (26) and a reaction involving oxidation of the nonglycyl carboxy group.

Filtering and drying of the precipitate after reflux followed by calcination at 600 °C or above results in a highly crystal-

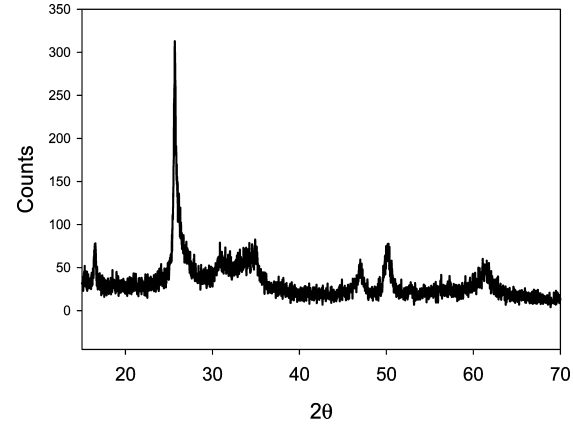

FIGURE 4. XRD data of a filtered and dried sample before calcination, indexing to $(NH_4)_2V_{10}O_{25}\cdot 8H_2O$.

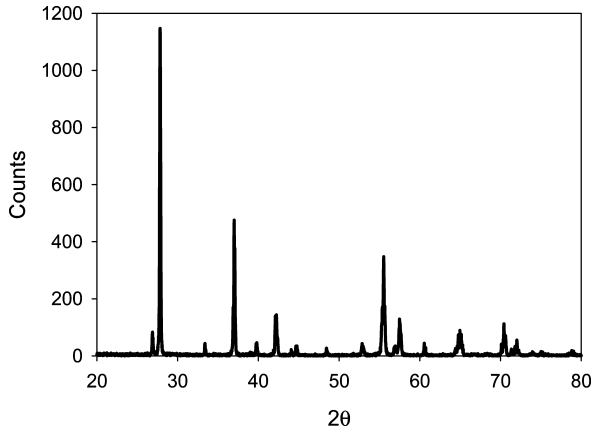

FIGURE 5. XRD data of a sample made from 0.9:1 aspartic acid/V_2O_5, refluxed for 2 h and calcined for 1 h at 800 °C.

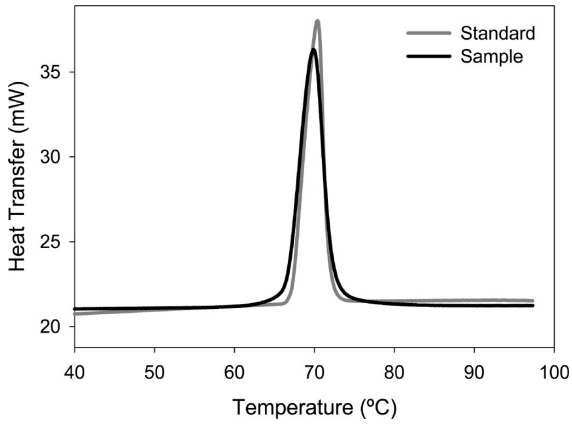

FIGURE 6. DSC data of a commercially available sample of VO_2 (Aldrich, 99.9%, black line) and a sample made from 0.9:1 aspartic acid/V_2O_5, refluxed for 2 h and calcined for 1 h at 800 °C (gray line).

line powder that exhibits the $P2_1/c$ symmetry of $VO_2(M_1)$ (1, 2), an example of which is presented in the XRD trace of Figure 5.

The enthalpy of the first-order phase transition can be used as an approximation for the purity of the material because the higher the enthalpy, the more VO_2 that is present, and therefore the higher the purity. The peak width also gives a good idea of the homogeneity of the sample, with a narrower, taller peak indicating reasonable purity and homogeneity, although subtle differences in the crystal grain sizes and defects may also affect the transition peak profile and area (28). However, as a first approximation, it is a useful comparison. Using a commercially available sample (99.9% VO_2, Aldrich) as a reference, Figure 6 presents a comparison of the DSC characterizations of both the commercial sample and that characterized in Figure 5. The commercial sample exhibits a transition temperature of 70.3 °C, while the aspartic acid generated sample peaks at 68.85 °C, in reasonable agreement. The phase transition enthalpy of the commercial sample is slightly lower than that of the aspartic acid generated sample: 39.67 J/g compared to 47.92 J/g, respectively. The peak profile of the commercial sample is noticeably sharper, and the broad base of the aspartic acid sample peak contributes significantly to the disparity in the total heat transfer. In general, the differences between the two profiles are small, and thus as an approximation the aspartic acid generated sample compares well with the commercial standard.

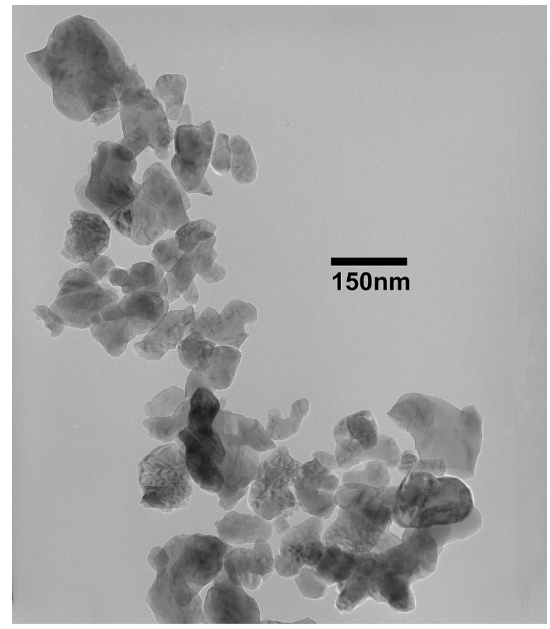

FIGURE 7. TEM image of the aspartic acid generated nanoparticles of Figure 6.

An electron micrograph of the aspartic acid generated VO_2 particles is presented in Figure 7, and the particles have a calculated mean diameter of approximately 90 nm. This is considerably smaller than the average primary particle size of the commercial sample, which is typically >10 μm, and may possibly be the origin of the discrepancies in the DSC data (28) because the smaller particle size, and therefore the crystallite size, results in a lower homogeneity of the lattice properties.

Vanadium Dioxide Composite Production. To form composites functionalization of substrate surfaces is required. However, it is practically quite difficult to calculate exactly the amount of amino acid needed for functionalization such that unwanted further reduction of the vanadium(IV) species occurs because the pure VO_2 synthesis is sensitive to the amount of amino acid added. Thus, a trial-and-error balance of the reducing and functionalizing amino acid amounts and reaction time needs to be struck.

The XRD and DSC results for a composite of VO_2 and SiO_2 using the above approach are presented in Figure 8a, b. The XRD data index to a single phase of $P2_1/c$ VO_2, with excellent intensities and no discernible impurities. The DSC data, however, while displaying a significant endothermic response, exhibit a small peak centered at 65 °C, followed by a much larger and broader peak centered at 73 °C. Integration of these two peaks gives a transition enthalpy of 51.0 J/g, which suggests that the degree of conversion of V_2O_5 to VO_2 is high and is confirmed by the very clean and intense XRD spectrum. However, the splitting and broadening of the DSC peak suggest that deposition onto surfaces may have some effect on the structure of VO_2 itself. It is well-known that the application of uniaxial stress on VO_2 can markedly

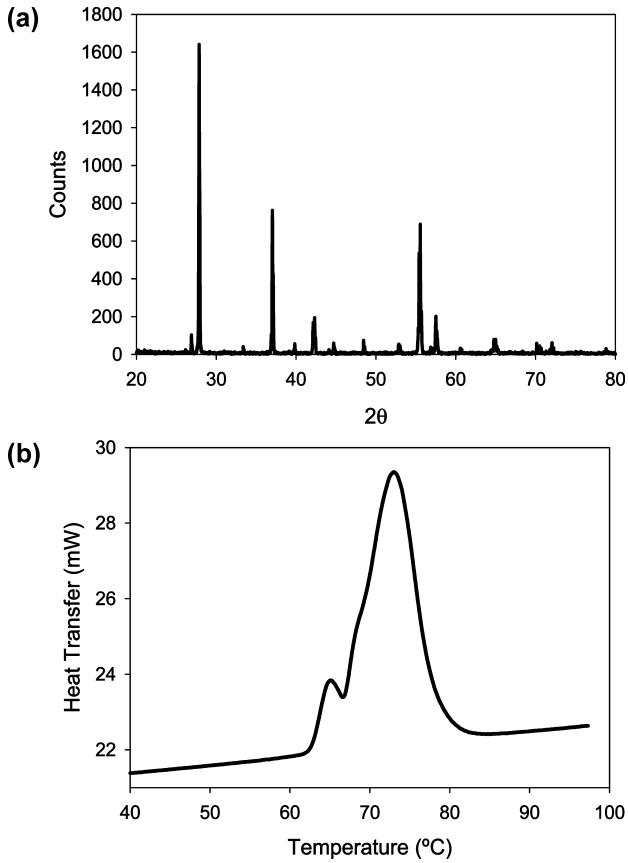

FIGURE 8. (a) XRD spectrum of a composite SiO_2/VO_2 sample indexing to monoclinic $P2_1/c$ (No. 14) VO_2. (b) DSC data of the SiO_2/VO_2 composite sample of part a. Integration of the area under both peaks gives a transition enthalpy of 51.0 J/g.

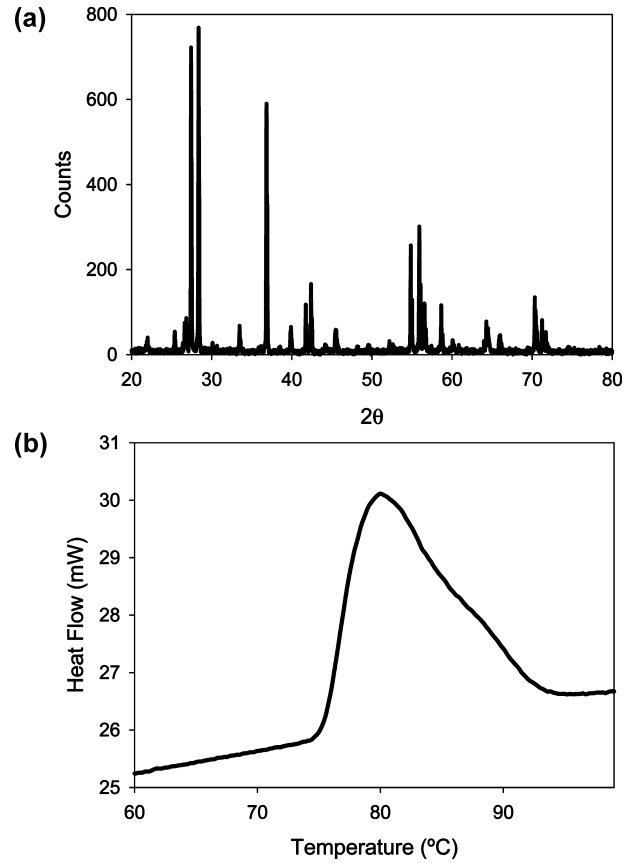

FIGURE 9. (a) XRD spectrum of a VO_2/montmorillonite composite, indexing to the M_2 $C2/m$ (No. 12) structure. (b) DSC data of a VO_2/montmorillonite composite that exhibits a first-order phase transition at 80.2 °C.

affect the crystal structure by disruption of the Peierls distortion (12), and it may be that alignment of the VO_2 crystal structure with that of a substrate may produce similar effects, a point to which we return later. However, the important message is that the crystal structure does not correlate well with phase transition dynamics. The splitting of the peak suggests the formation of a separate phase of VO_2 that is not influenced by the nature of the substrate. Given that the data of Figures 5 and 6 indicate that a third-party surface (in this case silica) is unnecessary for VO_2 formation, the presence of a phase that has not nucleated around the silica particles is unsurprising.

Serendipitously, it was discovered that a reduction reaction that had proceeded too far in the reflux stage, resulting in the production of mixtures of Magnéli (29) phases (V_nO_{2n-1}), could be reversed by centrifuging off the precipitate, redispersing, and aging it in water for an appropriate period of time. This allows some leeway in the amount of aspartic acid and reflux time used, and the Supporting Information illustrates the results of this process generating pure VO_2. Parts a and b of Figure 9 illustrate the results of this process for a VO_2/montmorillonite composite prepared as detailed above. However, the data, while indexing to a single phase of monoclinic VO_2, are actually characteristic of the structure of the M_2 intermediate phase (Figure 1b). The calorimetry data of Figure 9b exhibit the expected increase in the transition temperature, in line with data obtained for chromium-doped VO_2 in the M_2 structure (23).

As reflected in Figure 1a–c, the M_2 structure corresponds to an intermediate between the R and M_1 phases in which only one of the two chains of edge-sharing octahedra has undergone Peierls distortion. Thus, only half of the vanadium atoms form homopolar bonds with their neighbors, and therefore the shorter V–V distance is only half as frequent. This results in the M_1 (011), (210), and (022) peaks splitting into doublets, as Figure 9a illustrates. The question of how the M_2 phase formed preferentially may have an answer based on XAFS data and the data of VO_2 under uniaxial stress mentioned above (11, 12). The deposition of the vanadium(IV) oxide precursor during the reaction process is not expected to result in any preferential ordering of the vanadium oxide octahedra. It is the calcination process that arranges the precursor into crystalline VO_2. At a temperature of 800 °C, the amorphous vanadium oxide will be much more mobile than the crystalline montmorillonite platelets, and thus VO_2 can be thought of as being arranged around the montmorillonite during calcination. Therefore, the morphology of the substrate might be expected to significantly influence the ordering promoted by the high temperature. Given that stress along the [011] direction of the M_1 phase promotes the depairing of vanadium ions (12), templating (30) imposed by the platelet morphology of the montmorillonite surface may result in just such a stress, which may

therefore result in lattice hardening (11, 31), which affects the pairing of vanadium ions. These results suggest that VO_2 samples deposited on the surfaces of other materials may be affected by the surface morphology and lattice mismatching, and thus their properties in such states may differ from those of pure VO_2. Some significant advancements in the understanding of the MIT in VO_2 have recently come from measurements on films deposited on substrates (7), and the results herein suggest that substrate interaction must be taken into consideration via a comparison of the film and bulk powder transition dynamics.

CONCLUSION

A simple synthesis of the technologically significant material $P2_1/c$ (No. 14) VO_2 consisting of a reflux of vanadium pentoxide and aspartic acid in an aqueous solution has been presented. The method is capable of forming nanoparticles with phase transition characteristics and purity-matching those of a commercially available analytical-reagent-grade sample. The synthesis has the potential to decrease the cost of obtaining VO_2 by a factor greater than 10, with the added benefit of a primary particle size of approximately 90 nm. The reaction proceeds via the formation of a cross-linked network of vanadium(V) species, with aspartic acid forming the cross-links. Reduction of vanadium(V) occurs via a two-electron oxidation of amino acid and results in the precipitation of an amorphous vanadium(IV) precursor, which is converted to VO_2 via calcination. This gel-like intermediate is amenable to composite formation via binding to a substrate and results in the deposition of VO_2 onto the substrate surface. This solution-based deposition is unique to the synthesis reported and was used to form VO_2 on the surface of fumed silica particles; however, while the diffraction spectrum and phase transition enthalpy of the material indicated an M_1 VO_2 phase of high purity, the endothermic peak in the DSC spectrum split into a doublet of a small relatively narrow peak and a large broad peak. Deposition of VO_2 on the surfaces of montmorillonite particles resulted in the formation of a stable form of the intermediate M_2 phase of VO_2 without the need for doping with chromium (2) or the application of an external uniaxial stress (12), which has no literature precedent. Therefore, the synthesis described can be used to deposit high-purity VO_2 on the surfaces of other materials such as fumed silica and montmorillonite. However, the morphologies of the substrates were shown to have a significant impact on the dynamics of the structural phase transition. The results therefore suggest that, because static measurements of material properties (i.e., XRD) are not coincident with transition dynamics, more thorough (dynamic) comparisons of the sample properties with those of standards must be performed.

Acknowledgment. The authors gratefully acknowledge Dr. Weidong Yang for acquiring the DSC spectra and Dr. Russell Taylor for the indefinite loan of his voltammetry equipment.

Supporting Information Available: XRD data of a sample 0.9:1 (w/w) aspartic acid/V_2O_5, which was refluxed for 6 h and either calcined immediately (Figure S1) or centrifuged off and left to age in water for 16 h (Figure S2), showing a subsequent increase in homogeneity, and a DSC trace of the water-aged sample (Figure S3). This material is available free of charge via the Internet at http://pubs.acs.org.

REFERENCES AND NOTES

(1) Leroux, Ch.; Nihoul, G.; Van Tendeloo, G. *Phys. Rev. B* **1998**, *57* (9), 5111.
(2) Eyert, V. *Ann. Phys.* **2002**, *9*, 650.
(3) Wentzcovich, R. M.; Schulz, W. W.; Allen, P. B. *Phys. Rev. Lett.* **1994**, *72* (21), 3389.
(4) Woodley, S. M. *Chem. Phys. Lett.* **2008**, *453*, 167.
(5) Zylberstejn, A.; Mott, N. F. *Phys. Rev. B* **1975**, *11*, 4383.
(6) Paquet, D.; Leroux-Hugon, P. *Phys. Rev. B* **1980**, *22*, 5284.
(7) Qazilbash, M. M.; Brehm, M.; Chae, B.-G.; Ho, P.-C.; Adreev, G. O.; Kim, B.-J.; Yun, S. J.; Balatsky, A. V.; Maple, M. B.; Keilmann, F.; Kim, H.-T.; Basov, D. N. *Science* **2007**, *318*, 1750.
(8) Biermann, S.; Poteryaev, A.; Lichenstein, A. I.; Georges, A. *Phys. Rev. Lett.* **2005**, *94*, 026404.
(9) Haverkort, M. W.; Hu, Z.; Tanaka, A.; Reichelt, W.; Streltsov, S. V.; Korotin, M. A.; Anisimov, V. I.; Hsieh, H. H.; Lin, H.-J.; Chen, C. T.; Khomskii, D. I.; Tjeng, L. H. *Phys. Rev. Lett.* **2005**, *95*, 196404.
(10) Koethe, T. C.; Hu, Z.; Haverkort, M. W.; Schlüssler-Langeheine, C.; Venturini, F.; Brookes, N. B.; Tjernberg, O.; Reichelt, W.; Hsieh, H. H.; Lin, H.-J.; Tjeng, L. H. *Phys. Rev. Lett.* **2006**, *97*, 116402.
(11) Booth, J. M.; Casey, P. S. *Phys. Rev. Lett.* **2009**, *103*, 086402.
(12) Pouget, J. P.; Launois, H.; D'Haenens, J. P.; Merenda, P.; Rice, T. M. *Phys. Rev. Lett.* **1975**, *35* (13), 873.
(13) Berglund, C. N.; Guggenheim, H. J. *Phys. Rev.* **1969**, *185*, 1022.
(14) Manning, T. D.; Parkin, I. P.; Pemble, M. E.; Sheel, D.; Vernadou, D. *Chem. Mater.* **2004**, *16*, 744–749.
(15) Manning, T. D.; Parkin, I. P.; Clark, R. J. H.; Sheel, D.; Pemble, M. E.; Vernadou, D. *J. Mater. Chem.* **2002**, *12*, 2936.
(16) Wang, W.; Luo, Y.; Zhang, D.; Luo, F. *Appl. Opt.* **2006**, *45* (14), 3378–3381.
(17) Guiton, B. S.; Gu, Q.; Prieto, A. L.; Gudiksen, M. S.; Park, H. *J. Am. Chem. Soc.* **2005**, *127*, 498–499.
(18) Lu, S.; Hou, L.; Gan, F. *Thin Solid Films* **1999**, *353*, 40.
(19) Hanlon, T. J.; Coath, J. A.; Richardson, M. A. *Thin Solid Films* **2003**, *436*, 269–272.
(20) Xu, C.; Ma, L.; Liu, X.; Qiu, W.; Su, Z. *Mater. Res. Bull.* **2004**, *39*, 881.
(21) Shi, J.; Zhou, S.; You, B.; Wu, L. *Sol. Energy Mater. Sol. Cells* **2007**, *91* (19), 1856–1862.
(22) Peng, Z.; Jiang, W.; Liu, H. *J. Phys. Chem. C* **2007**, *111*, 1119–1122.
(23) Pan, M.; Zhong, H.; Wang, J. L.; Li, Z.; Chen, X.; Lu, W. *J. Cryst. Growth* **2004**, *265*, 121–126.
(24) Beteille, F.; Livage, J. *J. Sol—Gel Sci. Technol.* **1998**, *13*, 915–921.
(25) Booth, J. M.; Bhargava, S. K.; Bond, A. M.; O'Mullane, A. P. *J. Phys. Chem. B* **2006**, *110*, 12419–12426.
(26) Sherigawa, B. S.; Ishwar Bhat, K.; Pinto, I.; Made Gowda, N. M. *Int. J. Chem. Kinet.* **1995**, *27*, 675–690.
(27) Durupthy, O.; Bill, J.; Aldinger, F. *Cryst. Growth Des.* **2007**, *7*, 2696.
(28) Marega, C.; Marigo, A.; Causin, V.; Kapeliouchko, V.; di Nicoló, E.; Sanguineti, A. *Macromolecules* **2004**, *37*, 5630–5637.
(29) Schwingenschlögl, U.; Eyert, V. *Ann. Phys.* **2004**, *13* (9), 475–510.
(30) Doerner, M. F.; Nix, W. D. *CRC Crit. Rev. Solid State Phys. Mater. Sci.* **1988**, *14*, 225–268.
(31) Sun, L.; Chen, Y.-F.; He, L.; Ge, C.-Z.; Ding, D.-S.; Yu, T.; Zhang, M.-S.; Ming, N.-B. *Phys. Rev. B* **1997**, *55* (18), 12218.

AM900322B